NANO LETTERS

Letter

pubs.acs.org/NanoLett

Wedding Cake Growth Mechanism in One-Dimensional and Two-Dimensional Nanostructure Evolution

Xin Yin,[†] Jian Shi,[‡] Xiaobin Niu,[§,∥] Hanchen Huang,[§] and Xudong Wang*[,†]

[†]Department of Materials Science and Engineering, University of Wisconsin-Madison, Madison, Wisconsin 53706, United States

[‡]Department of Materials Science and Engineering, Rensselaer Polytechnic Institute, Troy, New York 12180, United States

[§]Department of Mechanical and Industrial Engineering, Northeastern University, Boston, Massachusetts 02115, United States

[∥]Institute of Fundamental and Frontier Science, State Key Laboratory of Electronic Thin Film and Integrated Devices, University of Electronic Science and Technology of China, Chengdu 610054, People's Republic of China

Supporting Information

ABSTRACT: The kinetic processes and atomistic mechanisms in nanostructure growth are of fundamental interest to nanomaterial syntheses with precisely controlled morphology and functionality. By programming deposition conditions at time domain, we observed the wedding cake growth mechanism in the formation of 1D and 2D ZnO nanostructures. Within a narrow growth window, the surfaces of the 1D and 2D structures were covered with a unique concentric terrace feature. This mechanism was further validated by comparing the characteristic growth rates to the screw dislocation-driven model. An interesting 1D to 2D morphology transition was also found during the wedding cake growth, when the adatoms overcome the Ehrlich−Schwoebel (ES) barrier along the edge of the top crystal facet triggered by lowering the supersaturation. The wedding cake model might be a general growth mechanism for flat-tipped nanowires that do not possess any dislocations. This study enriches our understanding on the fundamental kinetics of nanostructured crystal growth and provides a transformative strategy to achieve rational design and control of nanoscale geometry.

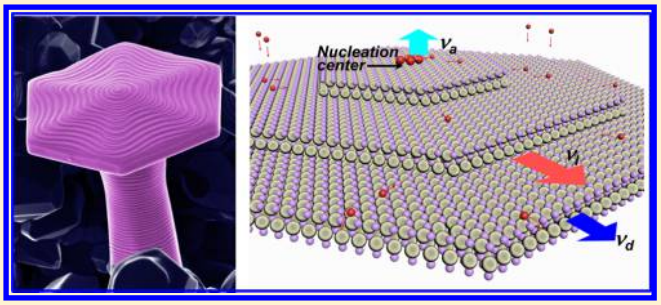

KEYWORDS: *Wedding cake mechanism, Ehrlich-Schwoebel barrier, zinc oxide, one-dimensional crystal growth, two-dimensional crystal growth*

Morphology is one essential element that gives rise to extraordinary physical, chemical, and mechanical properties in nanomaterials. Precise morphology control of nanomaterials is a notorious task, which heavily relies on fundamental understanding of the governing atomistic mechanisms and kinetics at the nanoscale. For decades, crystals with distinct and well-defined morphologies and dimensions, including quasi-one-dimensional (1D) nanowires (NWs) and two-dimensional (2D) nanosheets or nanoplates, have long been used as a model system to study crystal growth kinetics.[1−7] Generally, knowledge of thermodynamics and kinetics learned from materials growth in bulk systems still hold at nanoscale. Nevertheless, as interfacial free energy becomes substantial and atomic diffusion dimensions reduce drastically in nanoscale systems, the operation of these traditional bulk crystal growth principles in the world of nanomaterials may vary and in turn lead to vast difference in nanomorphology evolution. Despite numerous studies on the growth and application of nanostructures, current understanding of kinetics that governs the nanocrystal evolution is yet limited.

As a representative 1D nanostructure, NWs have been intensively studied for decades. Answering the question "How does a NW form?" has yielded many influential scientific insights to nanoscale crystal evolution kinetics, yet it is still an intriguing puzzle since many new observations cannot be fully and satisfactorily explained. In a homogeneous NW system where no foreign atoms are involved in the nucleation and growth, oriented attachment and screw dislocation-driven growth were proposed as representative growth mechanisms. The oriented attachment depicts the formation of 1D or 2D nanostructures through preferred stacking of preformed nanocrystals along their high-energy surfaces.[8−10] The screw dislocation-driven growth, long being known as a typical bulk crystal growth model, was also identified as an interpretation for NW formation.[5] Resent research highlighted a significant role of screw dislocations in the growth of various 1D and 2D structures including nanowires,[11−13] nanotubes,[14] and nanoplates.[15−19] Nevertheless, facing the great variety of nanoscale morphologies these two mechanisms many times are insufficient to explain a substantial portion of nanocrystal growth phenomena. In this paper, we report an observation of

Received: October 6, 2015
Published: October 26, 2015

DOI: 10.1021/acs.nanolett.5b04072
Nano Lett. 2015, 15, 7766−7772

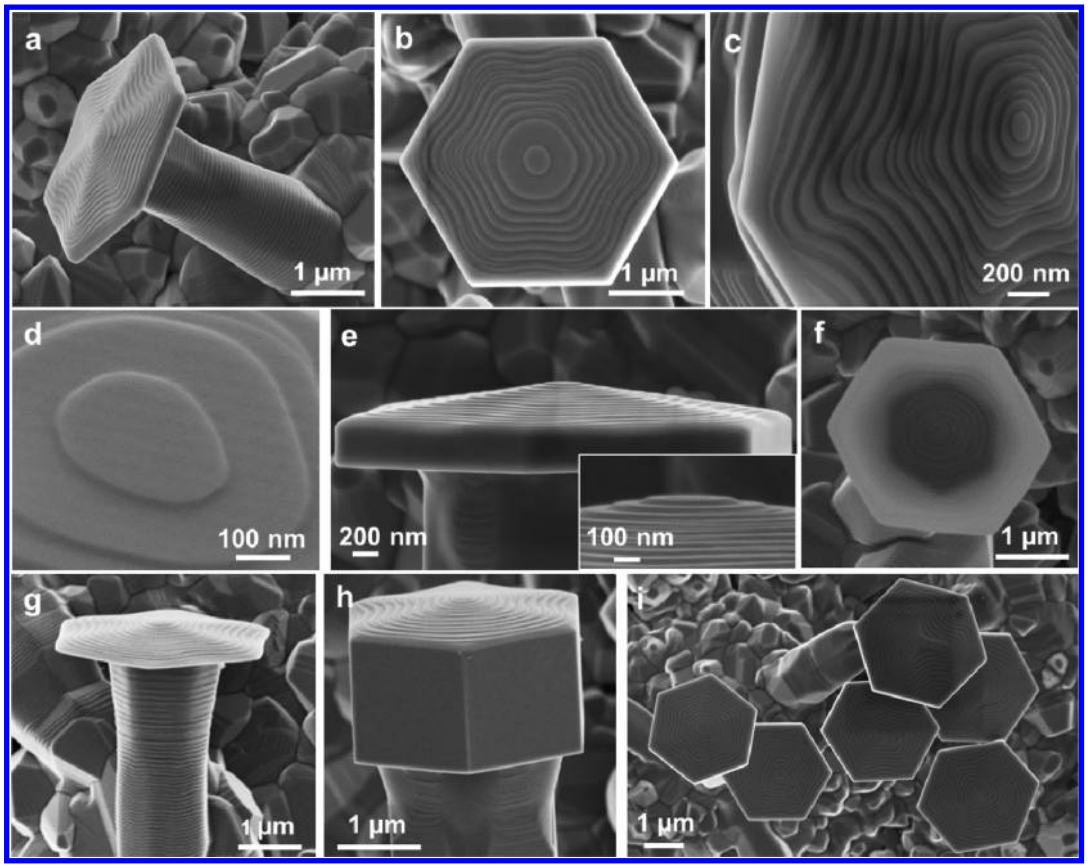

Figure 1. Morphology of microplate-caped micropillars. (a) An individual microplate-caped micropillar clearly shows a threadlike feature on both plate and pillar surfaces. (b) Top view of a microplate exhibiting a hexagonal outline with multiple concentric terrace circles. (c) Tilted and enlarged view of a microplate showing the intermediate subterraces extruding along the six equivalent corner directions. (d) A flat and smooth central terrace surface without any observable screw dislocation steps. (e) Side view of a microplate showing the terraced structure descending from the center of the plate. Inset shows the flat top terrace. (f) An image of a very thin microplate revealing orientation of the microplate and micropillar is differentiated by 30°. (g,h) Examples of plate-caped micropillars with small (g) and large (h) plate thicknesses. (i) Irregular terrace patterns due to the shadowing effect at high plate density region.

the wedding cake growth mechanism in the formation of 1D and 2D ZnO nanostructures. The wedding cake growth model yields a very similar terraced surface as that generated by a screw dislocation but does not possess a dislocation core and spiral pattern. An interesting 1D to 2D morphology transition was also found during the wedding cake growth, when the adatoms overcome the Ehrlich−Schwoebel (ES) barrier along the edge of the top crystal facet, triggered by lowering the supersaturation. Observation and investigation of the wedding cake growth model enriches our understanding of nanoscale crystal growth mechanisms, which could guide precise morphology design in nanosynthesis and manufacturing.

The unique ZnO microstructure was obtained under a dynamic deposition condition, where the growth chamber temperature was rapidly increased from room temperature to 1673 K within 90 min (Supporting Information Figure S1). During the ramp, both the Zn vapor concentration and the ZnO deposition temperature rose continuously. The ZnO microstructure composes a micrometer-sized pillar that was capped with a large hexagonal microplate (Figure 1a). The pillars were typically several micrometers long with a diameter of ∼1 μm. The microplates were ∼2−3 μm in diameter with variable thicknesses. A thread-like feature can be clearly observed both along the side of the pillar and on the plate surface. The top microplate exhibited a sharp hexagonal outline with multiple concentric terraces (Figure 1b). These terraces, however, did not exhibit a sharp hexagonal outline as the microplate showed, whereas extrusions together with intermediate subterraces (indication of rapid growth front) can be observed along the six equivalent corner directions (Figure 1c). Although this surface feature is very much similar to a screw dislocation growth pattern, a spiral center, which is the characteristic feature of a screw dislocation-driven growth, could not be observed. All the plates exhibited a flat and smooth central terrace surface (Figure 1d). This phenomenon fits well to the wedding cake growth model, where new atomic layers nucleate on the current top layer giving rise to a wedding cakelike structure. A side view of the plate clearly displays the stepwise terrace configuration (Figure 1e), indicating the terraces were evolved initially at the center and then spread out to the edge. A zoomed-in image also shows the flat top terrace without a spiral center (inset of Figure 1e).

From very thin plates that electrons can penetrate through, the orientation relationship between the plate and pillar can be observed. As shown in Figure 1f, the darker hexagon at the center of the plate outlines the pillar underneath. The hexagonal capping plate exhibited a 30° rotation in its orientation. On the basis of the crystallography of wurtzite ZnO (Supporting Information Figure S3), this feature suggests that the six equivalent side facets of the pillar and the plate are either one of the two low-energy surfaces of $\{01\bar{1}0\}$ and $\{11\bar{2}0\}$, respectively. The thickness of the plates exhibited a

DOI: 10.1021/acs.nanolett.5b04072
Nano Lett. 2015, 15, 7766−7772

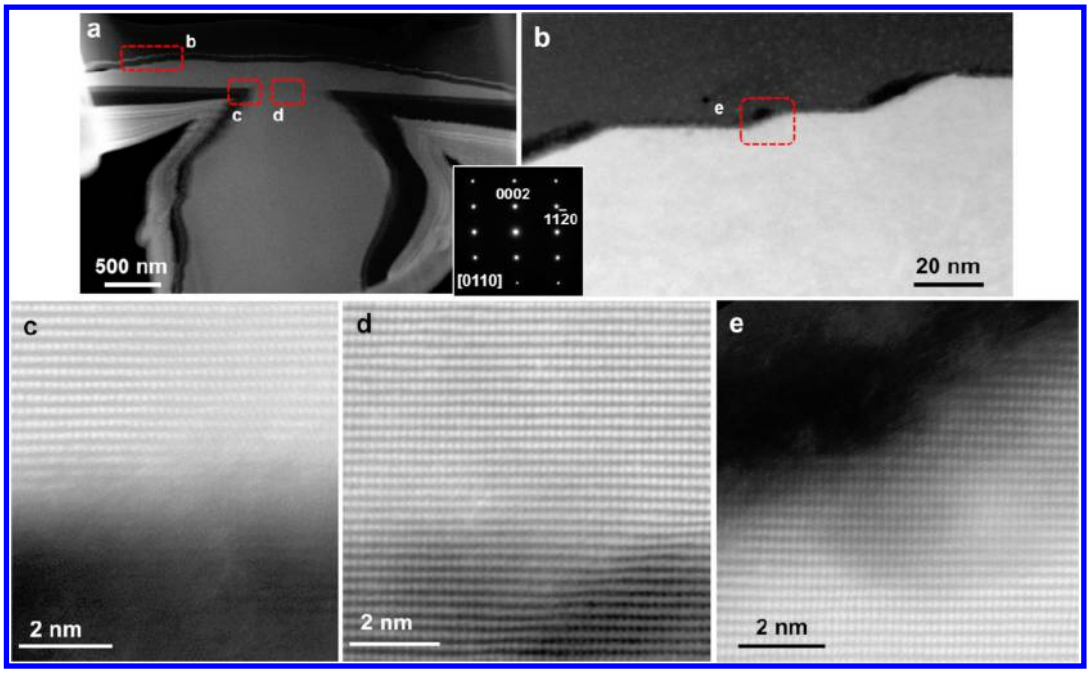

Figure 2. Crystal structure of microplate-caped micropillars. (a) Low-magnification STEM image of a cross-sectional slice of a plate-caped micropillar structure prepared by focused ion beam along the axial direction. The black intermedia layer is carbon and the outmost layer is platinum for protecting the structure from beam damage during sample preparation. Inset is the selective area electron diffraction pattern taken from the cross-sectional sample. (b) Enlarged terrace area as marked in panel a revealing the variation of terrace height was between 5 and 20 nm. (c) HR-STEM images of the plate-pillar joint corner showing the microplate and micropillar are a coherently grown single crystal. (d) HR-STEM image at the terrace center showing a perfect lattice without any dislocation. (e) HR-STEM image of the terrace edge revealing multiple small atomic steps.

large variation ranging from 50 nm to ∼1 μm (Figure 1g,h). Regardless of the thickness, all the plates had a very uniform width along their entire thickness with a clear convex terraced top surface. While most plates exhibited a six-fold symmetric terrace pattern, irregular terrace patterns could be observed at high density region (Figure 1i). Shadowing effect or competition of precursor might be responsible for the asymmetric growth behavior.

The crystal structure of ZnO plate-caped micropillars was characterized by Cs-corrected scanning transmission electron microscopy (STEM). Figure 2a shows a cross-sectional slice along the axial direction, where the ZnO structure was covered by carbon (the black intermedia layer) and platinum (the outmost layer) to protect it from ion beam damage during sample preparation. Selective area electron diffraction (SAED) pattern taken from the cross-sectional structure revealed that the entire structure was a single crystal and grew along the ⟨0001⟩ direction (inset of Figure 2a). The height of each terrace was in a range of 5−20 nm (Figure 2b). The terrace edge was not perpendicular to the plate surface and all of them showed a slope of ∼153°. These two features could be attributed to the step bunching effect during the monolayer propagation.[20] High-resolution STEM (HR-STEM) images taken at the plate-pillar joint region (Figure 2c,d for the corner and interface region, respectively) showed a coherent crystal lattice and no grain boundary or other dislocations could be found. Particularly, no indication of the existent of a screw dislocation core was discovered along the center position where the top terraces nucleated (Figure 2d). The terrace edge was found composed of multiple small steps without any dislocations, consistent with SEM observations (Figure 2e). The HRTEM observations further evidence that the wedding cake growth model governed the evolution of ZnO crystals.

Supported by microscopy observations, the wedding cake growth model with the step bunching effect is used to analyze the evolution of the 2D microplates. In a wedding cake growth, formation of surface terraces relies on nucleation of new atomic layers on the top surface due to the accumulation of concentrated adatoms confined by the energy barrier at step edges. This situation repeats yielding the representative morphology of concentric circular mounds without a spiral feature (Figure 3a). Although monoatomic layer step is the most common feature, multilayer terraces could also be obtained due to the step bunching effect when the ES barrier becomes negative.[20] The wedding cake growth behavior was mostly observed in the low-temperature epitaxial growth of metal surfaces.[21−23] However, in our hybrid structure, evolution of suspended 2D plates requires the lateral growth to exceed the supporting pillar's top surface. Therefore, adatoms need to overcome the ES barrier to diffuse down at the terrace edge[24,25] and then incorporate at the corner along the vertical facets. Lattice kinetic Monte Carlo (LKMC) method was used to simulate the morphology evolution when the ES barrier becomes tangible (Supporting Information S4). As shown in Figure 3b, under normal deposition condition a regular rod morphology was formed (panel i). As the supersaturation continuously decreases, the diffusion length of adatoms increases and therefore the attempting rate to jump over the edge increases.[26,27] However, the ES barrier blocks the adatoms from diffusing down. When the supersaturation drops to below a certain point, adatoms will attempt enough number of times to overcome the ES barrier to successfully diffuse down to the vertical facets and quickly nucleates an additional atomic layer circling around the tip of the rod (panel (ii)). As the growth continues, the plate becomes larger and thicker forming the final hybrid morphology (panel (iii)). This simulation verifies

DOI: 10.1021/acs.nanolett.5b04072
Nano Lett. 2015, 15, 7766−7772

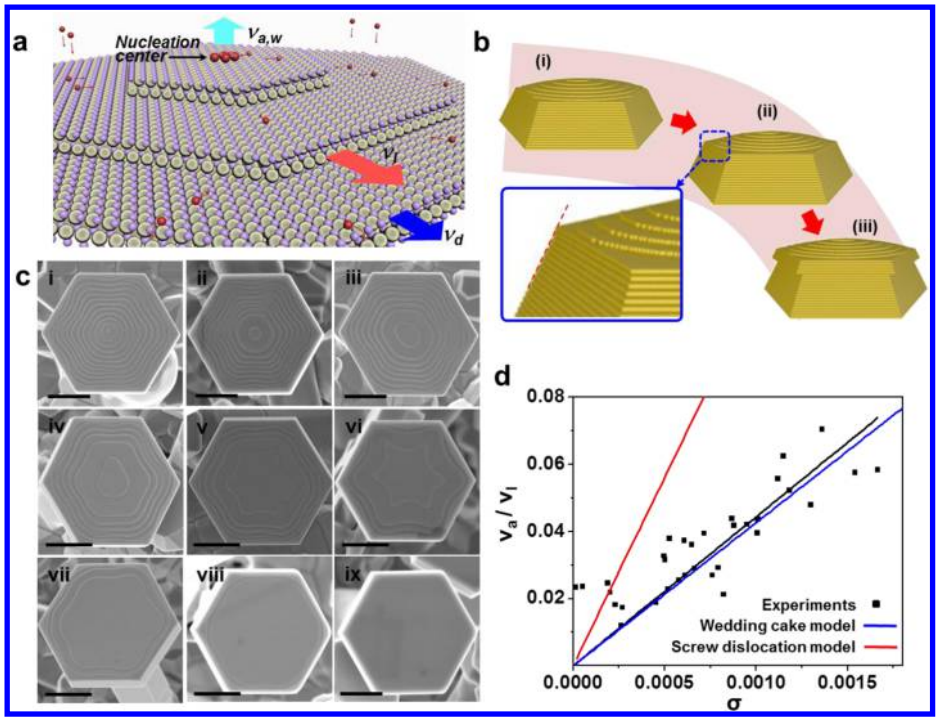

Figure 3. Wedding cake growth model. (a) Schematic of the wedding cake growth process. Oxygen atoms (white balls) and zinc atoms (purple balls) form the wurtzite structure. Red balls indicate the active adatoms diffusing on the terraces. $v_{a,w}$ is the axial growth rate, determined by the nucleation rate of new layers. v_l is the lateral growth rate, determined by the incorporation of adatoms to the side ledges of the terraces. v_d is the growth rate of the suspended plate area determined by the diffuse down rate of adatoms. (b) Kinetic Monte Carlo simulation results showing the 1D to 2D structure growth transition as a result of overcoming the ES barrier. (i) 1D growth of a rod structure at a relatively high supersaturation; (ii) appearance of the first atomic layer out of the rod surface when the supersaturation decreases to a certain point (inset shows an enlarged corner emphasizing the first atomic layer); (iii) continuous growth of the capping plate under favorable conditions. (c) Microplates with various numbers of terraces. The number of terraces decreased as the sampling point moved along the gas flow (downstream) direction. i–ix are microplate samples collected at position 16.8479, 16.8664, 16.8669, 16.9033, 16.9189, 16.9256, 16.9459, 16.9741, and 17.0129 cm from the center point, respectively. All the scale bars are 1 μm. (d) Plots of the axial to lateral growth rate ratio as a function of supersaturation. Black dots are measured data. Black line is the fitted curve based on the measured data, where a linear relationship can be determined. Blue line is derived from wedding cake growth model. Red line calculated is from screw dislocation growth model for comparison.

that the ES barrier triggers the formation of the suspended plate morphology.

To better understand the wedding cake growth mechanism in nanostructure evolution, numeric calculations were implemented to analyze the growth rates along different directions in comparison to the screw dislocation-driven growth mechanism. In a wedding cake growth, the lateral growth rate v_l is a measure of how fast adatoms attach to the ledge front, which is same as that in a screw dislocation growth. Quantitatively, for monolayer steps, $v_{l,mono}$ can be presented following the Burton–Cabrera–Frank (BCF) theory[5,28]

$$v_{l,\mathrm{mono}} = \frac{2\lambda_s \nu \exp\left(-\frac{\phi_{1/2}}{kT}\right)}{1 + \frac{\delta}{a}\exp\left(\frac{2\Delta U - E_{des}}{2kT}\right)}\sigma \quad (1)$$

where a is the distance between adsorption sites, ν is the vibration frequency, $\varphi_{1/2}$ is the work to detach an atom from half-crystal position to the vapor, k is the Boltzmann constant, T is temperature, σ is the supersaturation, λ_s is the mean free path of an adatom, δ is average spacing of the kink sites, ΔU is the kinetic barrier for the incorporation of the building units into the half crystal, and E_{des} is the desorption energy from the surface to the vapor. Bunched steps have a lower lateral velocity than monolayer steps due to the increased sites for the adatoms.[28] A rectification coefficient could be added to eq 1 to represent the growth rate change due to step bunching (Supporting Information S7.2).

As for the vertical growth rate v_a, in the wedding cake model it is directly related to the nucleation rate of new layers, which occurs only when the top terrace reaches a critical size.[26] Therefore, the axial growth rate can be formulated as[29]

$$v_{a,w} = \frac{h}{R_c} v_l \quad (2)$$

where R_c is the critical size of the top terrace and h is the height of the newly formed terrace, which could be either single or multiple atomic layer(s). On the other hand, the axial growth rate of the screw dislocation model follows the BCF theory

$$v_{a,s} = a\nu \exp\left(-\frac{\phi_{1/2}}{kT}\right)\frac{\sigma^2}{\sigma_c}\tanh\frac{\sigma_c}{\sigma} \quad (3)$$

where σ_c is characteristic supersaturation (Supporting Information S6). Because there is no nucleation involved in the screw dislocation growth, wedding cake model usually exhibits a slower vertical growth rate.[30]

One direct result of the different axial and lateral growth rates is the number of terraces on the plate surface. Within the deposition area (~2 mm in length) where terraced plates were received, the number of terraces decreased as the sampling point moved along the gas flow (downstream) direction,

DOI: 10.1021/acs.nanolett.5b04072
Nano Lett. 2015, 15, 7766–7772

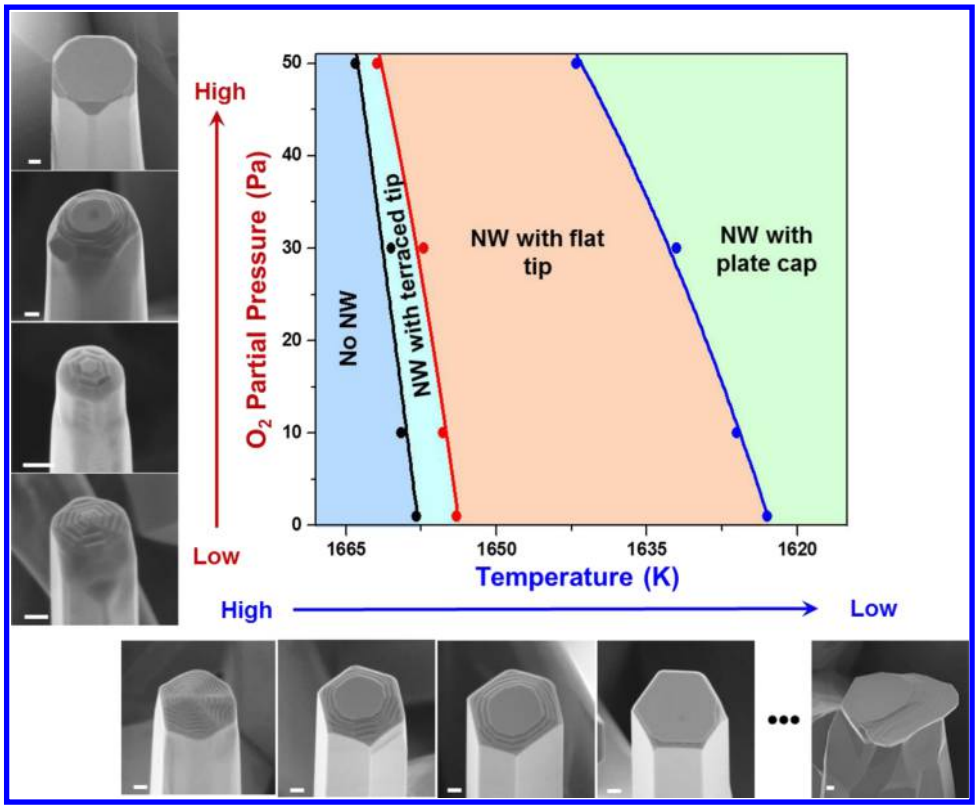

Figure 4. Nanowire morphology evolution with temperature and O_2 partial pressure. (Middle Panel) Quasi-phase diagram showing the 1D-to-2D morphology evolution in correlation to temperature and oxygen partial pressure. (Left Panel) Number of terraces decreases when increasing O_2 partial pressure. (Bottom Panel) Number of terraces decreases when decreasing the temperature and after a wide temperature range the microplate appeared under the oxygen partial pressure 50 Pa. All scare bars are 200 nm.

whereas no obvious size variation could be identified (Figure 3c). Statistical sampling showed that the number of terraces decreases monotonically with the distance (Supporting Information Figure S4). By assuming the time of evolving all the terraces equals to the growth time of the base terrace, the number of terraces was converted into the axial to lateral growth ratio (v_a/v_l, Supporting Information S7.2). Because the supersaturation is a function of the deposition location (Supporting Information S7.3), the relation between v_a/v_l and supersaturation was determined (Figure 3d). A linear relation was identified from the fitted curve with a slope of 44.4 (black line in Figure 3d). This relation shows that the v_a/v_l ratio increases with supersaturation, suggesting a trend that the number of terrace increases with supersaturation. The $v_{a,w}/v_l$ ratio was then derived based on the wedding cake growth model from individual microplates (Supporting Information S8), yielding a linear relation between $v_{a,w}/v_l$ and σ with a slope of 42.7 (blue curve). For comparison, $v_{a,s}/v_l$ as a function of σ was also calculated for the screw dislocation model by taking the ratio of eqs 1 and 3, yielding a slope of 112.4 (red curve). Here v_l is the monolayer step velocity. Considering bunched steps have a lower lateral velocity than that of monolayer steps, the $v_{a,s}/v_l$ ratio of bunched steps will be even higher than 112.4. The significantly closer match of the wedding cake model further evidence the governing role of the wedding cake mechanism in the evolution of ZnO microplate structure. It should be noted that v_l decreases as the terrace approaches the edge as evidenced by the denser terrace outlines near the edge (Figures 1b and 3c). This phenomenon could be attributed to the narrowing of the effective adatom collection area (Supporting Information S7.2)

In order to reveal the σ-related evolution of wedding cake tip morphology in a more general NW growth scenario, the deposition condition was adjusted to reach desired σ for NW formation (Supporting Information S9). Under this condition, ZnO NWs were formed with uniform size and geometry, where each NW exhibited a terraced tip feature (Supporting Information Figure S7). Just like the microplates, the central terrace exhibited a flat surface and no hint of the existence of any screw dislocation could be observed by both SEM and TEM characterizations (Supporting Information Figures S7 and S8). All the observations evidenced the wedding cake growth mechanism in the formation of these NWs. Furthermore, the tip terrace feature (number of terraces, Supporting Information Figures S8 and S9) exhibited the same relation with the deposition temperature as that observed from microplates. As shown in the bottom panel of Figure 4, when the deposition temperature decreases the number of terrace at the NW tip decreases and eventually the flat tip morphology was obtained. After a relative large temperature range, the suspended microplate morphology appeared, suggesting the deposition condition reached the critical low σ region. Similar change could also be observed by increasing the oxygen partial pressure. Qualitatively, high oxygen content in the reaction chamber hinders the decomposition of ZnO precursors and thus lowers σ. Therefore, as the oxygen partial pressure increased, the NW tip exhibited the similar change from a large number terraced surface to a flat tip, as shown in the left panel of Figure 4. The σ-related terrace evolution phenomenon was

DOI: 10.1021/acs.nanolett.5b04072
Nano Lett. 2015, 15, 7766−7772

further validated by implementing a very high supersaturation where $v_{a,w}$ catches up and exceeds v_l. Because of the rapid nucleation of new terraces, NWs with a narrow and long tapered tip were obtained (Supporting Information Figure S11).

From the oxygen partial pressure and deposition temperature relation, a quasi-phase diagram was constructed to show the evolution of terrace surfaces in both 1D and 2D morphologies (Figure 4). In general, a narrow range at high temperature was identified corresponding to the high-σ terraced region, where NWs with terraced tip were collected. NWs with regular flat tips could be found within a much wider temperature range. The flat-tipped NW morphology covers a relatively large supersaturation region, where the nanostructure growth condition could easily fall in. This might be the reason that flat-tipped NW structure was typically obtained.[31−33] The plate-caped NW morphology was collected in a further lower temperature zone, corresponding to the lowest σ for NW growth. All the boundaries between different morphologies shift to higher temperature as the oxygen partial pressure increases, because the reduction of σ due to raised oxygen content needs to be compensated by raising the deposition temperature.

In conclusion, the evolution of 2D plate structure from 1D pillars represents a dynamic crystal growth behavior transition when the local deposition conditions were tuned in situ. It lively recorded the wedding cake growth model in nanostructure formation from vapor phase, which was rare to be observed when the deposition conditions remained constant. The terrace feature on these nanostructures provided a valuable platform for understanding the wedding cake growth kinetics that could be an important mechanism to design and predict the nanocrystal morphology formation from the bottom-up. Analyzing the supersaturation and temperature-related growth behavior provides a new insight into nanostructure growth mechanisms and morphology control.

Methods. ZnO nanostructures were synthesized via vapor−solid deposition process. Five grams of ZnO powder was used as the precursor and placed at the center of an alumina tube in the furnace. Argon carrier gas with the flow rate of 50 sccm was applied and the pressure inside the tube was kept at 53 Pa. Alumina slices (11.4 cm in length and 1 cm width for each) were used as the substrates and placed downstream. The system temperature reached 1673 K after 90 min. Before the temperature reached 1673 K, the precursor completely vaporized. Subsequently, the system was cooled down to room temperature under the same atmosphere. For ZnO NW growth with the terraced feature at the tip, oxygen carrier gas with different flow rates of 0.5, 5, 15, and 25 sccm were used to adjust the growth kinetics. Top view and side view SEM images of the nanostructures were recorded directly from the as-synthesized substrates. For STEM of microplate-caped micropillars, the nanostructure was first transferred to the TEM grid using a micromanipulator, and focused ion beam was then used to cut the nanostructure into a thin slice. Detailed experimental procedures can be found in the Supporting Information.

■ ASSOCIATED CONTENT

Supporting Information

The Supporting Information is available free of charge on the ACS Publications website at DOI: 10.1021/acs.nanolett.5b04072.

More details on the sample synthesis and characterization, simulation method, growth rate calculation, and more analysis on SEM and TEM images. (PDF)

■ AUTHOR INFORMATION

Corresponding Author

*E-mail: xudong@engr.wisc.edu.

Author Contributions

X.W. conceived and supervised the project. X.Y. conducted the CVD growth. X.Y. and J.S. conducted the measurements. H.H. and X.N. conducted the simulation. X.W., X.Y., and J.S. wrote the manuscript. All authors discussed the results and commented on the manuscript.

Notes

The authors declare no competing financial interest.

■ ACKNOWLEDGMENTS

The authors thank financial support from Air Force Office of Scientific Research under Award FA9550-13-1-0168 and National Science Foundation under Award CMMI-1148919. X.N. and H.H. acknowledge the financial support from Department of Energy Office of Basic Energy Sciences (DE-FG02-09ER46562).

■ REFERENCES

(1) Geohegan, D. B.; Puretzky, A. A.; Jackson, J. J.; Rouleau, C. M.; Eres, G.; More, K. L. *ACS Nano* **2011**, *5* (10), 8311−8321.
(2) Hu, J. T.; Ouyang, M.; Yang, P. D.; Lieber, C. M. *Nature* **1999**, *399* (6731), 48−51.
(3) Chou, Y. C.; Hillerich, K.; Tersoff, J.; Reuter, M. C.; Dick, K. A.; Ross, F. M. *Science* **2014**, *343* (6168), 281−284.
(4) Wagner, R. S.; Ellis, W. C. *Appl. Phys. Lett.* **1964**, *4* (5), 89−90.
(5) Burton, W. K.; Cabrera, N.; Frank, C. *Philos. Trans. R. Soc., A* **1951**, *243* (866), 299−358.
(6) Kossel, W. *Nachr. Ge. Wiss. Göttingen, Math.-Phys. Kl.* **1927**, *1927*, 135−143.
(7) Stranski, I. *Z. Phys. Chem.* **1928**, *136* (259), 259−278.
(8) Penn, R. L.; Banfield, J. F. *Science* **1998**, *281* (5379), 969−971.
(9) Shi, J.; Li, Z.; Kvit, A.; Krylyuk, S.; Davydov, A. V.; Wang, X. *Nano Lett.* **2013**, *13* (11), 5727−5734.
(10) Schliehe, C.; Juarez, B. H.; Pelletier, M.; Jander, S.; Greshnykh, D.; Nagel, M.; Meyer, A.; Foerster, S.; Kornowski, A.; Klinke, C.; Weller, H. *Science* **2010**, *329* (5991), 550−553.
(11) Meng, F.; Morin, S. A.; Forticaux, A.; Jin, S. *Acc. Chem. Res.* **2013**, *46* (7), 1616−1626.
(12) Bierman, M. J.; Lau, Y. K. A.; Kvit, A. V.; Schmitt, A. L.; Jin, S. *Science* **2008**, *320* (5879), 1060−1063.
(13) Zhu, J.; Peng, H.; Marshall, A. F.; Barnett, D. M.; Nix, W. D.; Cui, Y. *Nat. Nanotechnol.* **2008**, *3* (8), 477−481.
(14) Morin, S. A.; Bierman, M. J.; Tong, J.; Jin, S. *Science* **2010**, *328* (5977), 476−480.
(15) Morin, S. A.; Forticaux, A.; Bierman, M. J.; Jin, S. *Nano Lett.* **2011**, *11* (10), 4449−4455.
(16) Wang, F.; Seo, J.-H.; Ma, Z.; Wang, X. *ACS Nano* **2012**, *6* (3), 2602−2609.
(17) Wang, F.; Jakes, J. E.; Geng, D.; Wang, X. *ACS Nano* **2013**, *7* (7), 6007−6016.
(18) Forticaux, A.; Dang, L.; Liang, H.; Jin, S. *Nano Lett.* **2015**, *15*, 3403.
(19) Zhuang, A.; Li, J.-J.; Wang, Y.-C.; Wen, X.; Lin, Y.; Xiang, B.; Wang, X.; Zeng, J. *Angew. Chem., Int. Ed.* **2014**, *53* (25), 6425−6429.
(20) Krishnamurthy, M.; Wassermeier, M.; Williams, D. R. M.; Petroff, P. M. *Appl. Phys. Lett.* **1993**, *62* (16), 1922−1924.
(21) Henzler, M. *Surf. Sci.* **1993**, *298* (2−3), 369−377.

DOI: 10.1021/acs.nanolett.5b04072
Nano Lett. 2015, 15, 7766−7772

(22) Vrijmoeth, J.; Vandervegt, H. A.; Meyer, J. A.; Vlieg, E.; Behm, R. J. *Phys. Rev. Lett.* **1994**, *72* (24), 3843−3846.
(23) Bromann, K.; Brune, H.; Roder, H.; Kern, K. *Phys. Rev. Lett.* **1995**, *75* (4), 677−680.
(24) Ehrlich, G.; Hudda, F. G. *J. Chem. Phys.* **1966**, *44* (3), 1039−1049.
(25) Schwoebel, R. L.; Shipsey, E. J. *J. Appl. Phys.* **1966**, *37* (10), 3682−3686.
(26) Tersoff, J.; Vandergon, A. W. D.; Tromp, R. M. *Phys. Rev. Lett.* **1994**, *72* (2), 266−269.
(27) Niu, X.; Stagon, S. P.; Huang, H.; Baldwin, J. K.; Misra, A. *Phys. Rev. Lett.* **2013**, *110* (13), 136102.
(28) Markov, I. V.*Crystal Growth For Beginners: Fundamentals of Nucleation, Crystal Growth and Epitaxy*; World Scientific: Singapore, 2003.
(29) Krug, J. *Phys. A* **2002**, *313* (1−2), 47−82.
(30) Redinger, A.; Ricken, O.; Kuhn, P.; Raetz, A.; Voigt, A.; Krug, J.; Michely, T. *Phys. Rev. Lett.* **2008**, *100* (3), 035506.
(31) Wu, J. J.; Liu, S. C. *Adv. Mater.* **2002**, *14* (3), 215−218.
(32) Yao, B. D.; Chan, Y. F.; Wang, N. *Appl. Phys. Lett.* **2002**, *81* (4), 757−759.
(33) Liu, X.; Wu, X. H.; Cao, H.; Chang, R. P. H. *J. Appl. Phys.* **2004**, *95* (6), 3141−3147.

DOI: 10.1021/acs.nanolett.5b04072
Nano Lett. 2015, 15, 7766−7772